


## Reexamining the ground state and magnetic properties of curium dioxide

Li Huang,<sup>\*</sup> Ruofan Chen, and Haiyan Lu 

*Science and Technology on Surface Physics and Chemistry Laboratory, P.O. Box 9-35, Jiangyou 621908, China*



(Received 6 March 2020; revised 30 June 2020; accepted 28 July 2020; published 13 August 2020)

The ground-state electronic structure and magnetic behaviors of curium dioxide ( $\text{CmO}_2$ ) are controversial. In general, the formal valence of Cm ions in  $\text{CmO}_2$  should be tetravalent. The tetravalent state implies a  $5f^{6.0}$  electronic configuration and a nonmagnetic ground state. However, it is in sharp contrast to the large magnetic moment measured by painstaking experiments. In order to clarify this contradiction, we tried to study the ground-state electronic structure of  $\text{CmO}_2$  by means of a combination of density functional theory and dynamical mean-field theory. We find that  $\text{CmO}_2$  is a wide-gap charge transfer insulator with a strong  $5f$  valence state fluctuation. It indeed belongs to a mixed-valence compound. The predominant electronic configurations for Cm ions are  $5f^{6.0}$  and  $5f^{7.0}$ . The resulting magnetic moment agrees quite well with the experimental value. Therefore, the magnetic puzzle in  $\text{CmO}_2$  can be appropriately explained by the mixed-valence scenario.

DOI: [10.1103/PhysRevB.102.085127](https://doi.org/10.1103/PhysRevB.102.085127)

### I. INTRODUCTION

Actinide-based materials manifest complex and fascinating magnetic behaviors [1]. Recognizing them and understanding their underlying mechanisms are always hot topics in condensed-matter science. In the early actinides (such as U, Np, and Pu), itinerant  $5f$  electrons result in significant band dispersions and large bandwidths. Hence, the ratio between exchange interaction and  $5f$  bandwidth does not meet the requirement of the Stoner criterion [2], so magnetic ordering is absent in these actinides [3]. As for the late actinides (such as Am, Cm, Bk, and beyond), the picture is conspicuously different. The  $5f$  electrons in the late actinides should become localized. They are capable of spin polarization and realizing some kinds of magnetic ordering states. However, no macroscopic moment has been observed experimentally in Am [4]. This is because its orbital and spin moments are equal but have opposite signs ( $\mu_L = -\mu_S$ ). As a consequence, Cm comes to be the first actinide element that exhibits magnetic ordering under ambient conditions [5]. It has an antiferromagnetic ground state with a large ordered moment  $\mu_{\text{eff}} \approx 7.58\mu_B$  [6,7].

Now let us focus on the actinide dioxides,  $\text{AO}_2$ , which crystallize in a cubic  $\text{CaF}_2$ -like structure. They usually show complicated magnetic ordering phases and thus garner much attention [8]. In the early members of the actinide dioxides,  $\text{UO}_2$  and  $\text{NpO}_2$  are two striking examples.  $\text{UO}_2$  realizes a transverse  $3q$  magnetic dipolar and a  $3q$  electric quadrupolar order [9,10], while  $\text{NpO}_2$  is characterized by a high-rank magnetic multipolar order [11,12]. In the late members of the actinide dioxides,  $\text{PuO}_2$  is nonmagnetic due to its  $5f^{4.0}$  electronic configuration [13].  $\text{AmO}_2$  is supposed to have a longitudinal  $3q$  high-rank multipolar ordered state [14], similar to  $\text{NpO}_2$ . The magnetic behaviors in these actinide

compounds can be more or less explained theoretically. However, the magnetic properties of  $\text{CmO}_2$  are totally unexpected and have remained unsolved up to now [8].

Based on the ionic picture, it is generally accepted that the valences of actinide ions in actinide dioxides are tetravalent. We thus naively reckon that the Cm ions in  $\text{CmO}_2$  obey this rule as well. Note that there are six  $5f$  electrons for the  $\text{Cm}^{4+}$  ion. According to Hund's rules, the ground state of  $\text{Cm}^{4+}$  ion should be a singlet with  $J = 0$ ,  $S = 3$ , and  $L = 3$ . Undoubtedly, it is a nonmagnetic state. However, the temperature dependence of the magnetic susceptibility demonstrated a large effective moment of  $3.4\mu_B$ , and the analysis of the neutron diffraction pattern established that the  $\text{CmO}_2$  sample was no long-range magnetic order [15]. At first glance, the nonmagnetic ground state is inconsistent with the experimental results. In order to resolve this contradiction, several mechanisms have been proposed. A straightforward explanation is to consider the effect of  $\text{Cm}^{3+}$  magnetic impurity, which has seven  $5f$  electrons [16]. Its ground-state multiplet is characterized by  $J = 7/2$ ,  $S = 7/2$ , and  $L = 0$ . However, this explanation is already excluded by previous experiments. First, the samples are proven to be very close to stoichiometry. Second, if there is a mixture of  $\text{Cm}^{3+}$  and  $\text{Cm}^{4+}$ , the oxygen sublattice should be rearranged. But there is no experimental evidence for the corresponding superlattice peak in neutron diffraction spectra [15]. Another possibility to understand this problem is to consider the magnetic excited state of the  $\text{Cm}^{4+}$  ions [17]. Due to the interplay of Coulomb interactions, spin-orbit coupling, and crystalline electric field, the excitation energy is likely to be smaller than the value of Landé's internal rule. Consequently, Niikura and Hotta suggested that with carefully chosen parameters, the magnetic behaviors of  $\text{CmO}_2$  can be well reproduced by solving an Anderson impurity model [18]. They concluded that the effective magnetic moment should reduce with a decrease of the temperature. Once the temperature is low enough, the magnetic behaviors should disappear. This mechanism has not

<sup>\*</sup>lihuang.dmft@gmail.com

been confirmed by experiments. In addition to the two proposals, Prodan *et al.* suggested a covalent picture for  $\text{CmO}_2$ . In this picture, Cm could borrow electrons from O  $2p$  orbitals to achieve the stable half-filled  $5f$ -shell configuration [19]. They performed screened hybrid functional calculations. But the calculated lattice parameter deviates considerably from the measured value, and the obtained  $5f$  occupancy is only 6.2, which is too small to support the experimental magnetic moment.

Besides these puzzling magnetic behaviors,  $\text{CmO}_2$  has already distinguished itself from the other actinide dioxides for its intriguing ground-state properties. For example, the lattice constants for  $\text{AO}_2$  decrease monotonically with increasing atomic number [20]. However, the lattice constants in  $\text{CmO}_2$  deviate from this general trend obviously [21,22]. A cusp is noticed at  $\text{CmO}_2$  in the plot of the  $\text{AO}_2$  lattice constants  $a_0$  vs atomic number  $Z$  [19]. Another example is the single-particle properties of  $\text{CmO}_2$ . The actinide dioxides are usually charge-transfer insulators or Mott-Hubbard insulators with large band gaps ( $E_{\text{gap}} > 1$  eV) [8]. However, the band gap of  $\text{CmO}_2$  has not been determined experimentally, but most theoretical calculations have predicted a very small band gap ( $E_{\text{gap}} \sim 0.4$  eV) [19,23].

Apparently, not only the magnetic behaviors but also the ground-state electronic structure of  $\text{CmO}_2$  remain mysterious. In the present work, we would like to address these problems and propose a mechanism to explain its magnetic puzzle. We endeavor to study the ground-state electronic structure of  $\text{CmO}_2$  by means of a state-of-the-art first-principles many-body approach. Our results imply that the oxidation state of Cm ions in  $\text{CmO}_2$  is probably noninteger. In other words, it is neither  $\text{Cm}^{3+}$  [i.e., Cm (III)] nor  $\text{Cm}^{4+}$  [i.e., Cm (IV)]. Instead, it is mixed valence with a heavy  $5f$  valence state fluctuation. The  $5f$  electrons fluctuate among various electronic configurations (mainly  $5f^{6.0}$  and  $5f^{7.0}$ ) and thus lead to a sizable magnetic moment.

The rest of this paper is organized as follows. In Sec. II, the methodology and computational details are introduced briefly. Section III is the major part of this paper. All of the calculated results are presented there. In Sec. IV, we make a detailed comparison of the available mechanisms which could explain the magnetic moment of  $\text{CmO}_2$ . In addition, we further discuss the influence of temperature and pressure effects on the electronic structure of  $\text{CmO}_2$ . Finally, Sec. V provides a short summary.

## II. METHOD

In  $5f$  electronic systems, both Coulomb interactions and spin-orbit coupling play vital roles [1]. Therefore, it is essential to take them into consideration on the same footing [25]. In the present work, we employed the dynamical mean-field theory, in combination with the density functional theory (dubbed DFT + DMFT) to accomplish this job [26,27].

We utilized the WIEN2K software package [28], which implements a full-potential linearized augmented plane-wave formalism, to carry out the band structure calculations. The experimental crystal structure of  $\text{CmO}_2$  was used [21,22,29]. The generalized gradient approximation, specifically the Perdew-Burke-Ernzerhof functional [30], was selected to

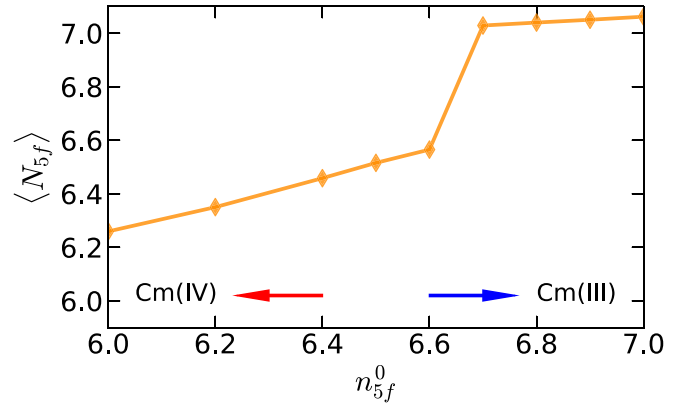


FIG. 1. Total  $5f$  occupancy  $\langle N_{5f} \rangle$  as a function of nominal  $5f$  occupancy  $n_{5f}^0$ .  $\langle N_{5f} \rangle$  is measured by the CT-HYB impurity solver [24]. See text for more details.

describe the exchange-correlation potential. The spin-orbit coupling was included. The  $K$  mesh for Brillouin zone integration was  $17 \times 17 \times 17$ , and  $R_{\text{MT}}K_{\text{MAX}} = 8.0$ . The muffin-tin radii for Cm and O ions were 2.5 and 1.7 au, respectively.

The strong correlated nature of Cm's  $5f$  electrons was treated in a nonperturbed manner by DMFT. We adopted the EDMFT software package, which was implemented by Haule *et al.* [31]. The Coulomb interaction matrix for Cm's  $5f$  electrons was parameterized by applying the Slater integrals  $F^{(k)}$ . The Coulomb repulsion interaction parameter  $U$  and Hund's exchange interaction parameter  $J_{\text{H}}$  were 7.5 and 0.6 eV, respectively [1]. The double-counting term for  $5f$  self-energy functions was subtracted via the fully localized limit scheme [32]. The expression reads

$$\Sigma_{\text{dc}} = U \left( n_{5f}^0 - \frac{1}{2} \right) - \frac{J_{\text{H}}}{2} (n_{5f}^0 - 1.0), \quad (1)$$

where  $n_{5f}^0$  denotes the nominal  $5f$  occupation number. In the present work, we tried various  $n_{5f}^0$  ( $n_{5f}^0 \in [6.0, 7.0]$ ) to mimic the different oxidation states of Cm ions (see Fig. 1). For instance, for Cm(IV),  $n_{5f}^0 = 6.0$ , while for Cm(III),  $n_{5f}^0 = 7.0$  [33]. Notice that  $n_{5f}^0$  is just an artificial parameter; it should not be altered during the calculations (see the Appendix). The hybridization expansion continuous-time quantum impurity solver (dubbed CT-HYB) [24,34,35] was employed to solve the resulting 14-band Anderson impurity models. The number of quantum Monte Carlo sweeps was  $2 \times 10^8$  per CPU process. The system temperature was approximately 116 K ( $\beta = 1/T = 100.0$ ), and the system was restricted to be paramagnetic [36]. We performed fully charge self-consistent DFT + DMFT calculations. The number of DFT + DMFT iterations was about 60–80.

## III. RESULTS

### A. Bulk properties

Previous attempts to apply the *ab initio* methods to study actinide-based materials have been hampered by the lack of highly accurate and efficient first-principles approaches that can correctly capture and describe the correlated nature of  $5f$  electrons. Although DFT + DMFT might be one of the most

TABLE I. Bulk properties, including equilibrium lattice constants  $a_0$  (Å), the bulk modulus  $B$  (GPa) and its first derivative with respect to the pressure  $B'$ , and band gap  $E_{\text{gap}}$  (eV), of  $\text{CmO}_2$ . Here, the phrases SOC, HSE, and SIC denote spin-orbit coupling, Heyd-Scuseria-Ernzerhof screened hybrid functional, and self-interaction correction, respectively.

	DFT + DMFT <sup>a</sup>	DFT + DMFT <sup>b</sup>	DFT + $U$ + SOC <sup>c</sup>	DFT + $U$ + SOC <sup>d</sup>	DFT + $U$ + SOC <sup>e</sup>	HSE <sup>f</sup>	HSE + SOC <sup>f</sup>	SIC <sup>g</sup>	Expt. <sup>h</sup>
$a_0$	5.45	5.42	5.410	5.523	5.490	5.365	5.360	5.37	5.359
$B$	223.1	235.5	193.3	129.6	123.7			212.0	218.0
$B'$	4.35	1.52	4.4	4.7	5.6				7.0
$E_{\text{gap}}$	3.5	1.8	1.94	metallic	metallic	0.4	0.4	0.4	

<sup>a</sup>The present work, Cm(III) case.

<sup>b</sup>The present work, Cm(IV) case.

<sup>c</sup>For the nonmagnetic state of  $\text{CmO}_2$ . See Ref. [23].

<sup>d</sup>For the ferromagnetic state of  $\text{CmO}_2$ . See Ref. [23].

<sup>e</sup>For the antiferromagnetic state of  $\text{CmO}_2$ . See Ref. [23].

<sup>f</sup>For the antiferromagnetic state of  $\text{CmO}_2$ . See Ref. [8].

<sup>g</sup>For the antiferromagnetic state of  $\text{CmO}_2$ . See Ref. [40].

<sup>h</sup>See Refs. [29,41].

powerful approaches ever established to study strongly correlated electron materials [26,27], it has seldom been applied to the late actinides and their compounds [25,37,38]. Here in order to build confidence in the DFT + DMFT approach, we tried to calculate the equilibrium properties, including lattice constants  $a_0$  and bulk modulus  $B$  of  $\text{CmO}_2$ . We at first calculated the  $E$ - $V$  curve and then used the Birch-Murnaghan equation of states [39] to fit it. Our results, together with the other theoretical and experimental values where available, are summarized in Table I.

It is clear that our results agree closely with the experimental and other theoretical values. For the Cm(III) case, the deviations are only  $\sim 1.7\%$  for  $a_0$  and  $\sim 2.3\%$  for  $B$ . As for the Cm(IV) case and the other potential oxidation states (not shown in Table I), the deviations are similar or even smaller. These facts suggest that the bulk properties of  $\text{CmO}_2$  are very well reproduced by the DFT + DMFT approach, irrespective of the oxidation states of Cm ions. Actually, Cm ions were assumed to be Cm(IV) in most of the previous theoretical calculations [8,40].

## B. Quasiparticle band structures

The quasiparticle band structures or momentum-resolved spectral functions  $A(\mathbf{k}, \omega)$  of  $\text{CmO}_2$  within various oxidation states [Cm(IV), the intermediate configuration ( $n_{5f}^0 = 6.5$ ), and Cm(III)] are depicted in Figs. 2(a), 2(d) and 2(g). The following characteristics are noticeable: (i) All figures show considerable band gaps (see Table I). Note that the band gap of the Cm(III) case is much larger than those of the other cases. This is not surprising because when the correlated orbital is half filled, it will suffer a larger effective interaction. This rule has been revealed in strongly correlated  $d$ -electron systems and model Hamiltonian calculations [42]. (ii) The band gaps of the Cm(IV) case and the intermediate configuration are indirect ( $\Gamma \rightarrow K$ ), which is consistent with the previous theoretical results [14,23,43]. Interestingly, the band gap of the Cm(III) case is direct. (iii) We observe stripelike patterns in these figures. These features exist at approximately  $-3 \text{ eV} < \omega < -1 \text{ eV}$  and  $\omega > 2 \text{ eV}$  for the Cm(IV) case,  $-4 \text{ eV} < \omega < -1 \text{ eV}$  for the intermediate configuration, and  $\omega < -1.5 \text{ eV}$  for the Cm(III) case. (iv) In addition, we also

observe narrow and flat bands in the vicinity of 0.4 and 2.0 eV for the intermediate configuration. The stripelike patterns and flat bands are mainly from the contributions of localized  $5f$  electrons. These  $5f$  bands look quite blurred, which indicates that the  $5f$  electrons are incoherent.

From the total density of states  $A(\omega)$  and  $5f$  partial density of states  $A_{5f}(\omega)$ , we can see that the band gaps are associated not only with the transitions between occupied and unoccupied  $5f$  states but also with the transitions between  $5f$  and other weakly correlated or noncorrelated orbitals [see Figs. 2(b), 2(e) and 2(h)]. According to the results of the three representative configurations, we can establish that  $\text{CmO}_2$  is a typical charge transfer insulator with a sizable band gap ( $> 1 \text{ eV}$ ), instead of Mott-Hubbard insulator. Previous theoretical studies predicted that  $\text{CmO}_2$  is a charge transfer insulator, but with a small band gap ( $< 1 \text{ eV}$ ) or even a semimetal [8,14,23,40]. To validate these predictions, further photoemission or optical experiments are highly desired [44].

From Fig. 2(a), significant overlaps exist between the  $5f$  bands and  $spd$  conduction bands between  $-3$  and  $-1 \text{ eV}$ . This means that there must be strong  $c$ - $f$  hybridization for the Cm(IV) case. For the intermediate configuration, strong  $c$ - $f$  hybridization is seen between  $-4$  and  $-1 \text{ eV}$  [see Fig. 2(d)]. For the Cm(III) case, a similar phenomenon is observed when  $\omega < 1.5 \text{ eV}$  [see Fig. 2(g)]. Note that the  $5f$  hybridization function  $\Delta(\omega)$  is an ideal measurement for the  $c$ - $f$  hybridization effect. In Figs. 2(c), 2(f) and 2(i), the  $5f$  hybridization functions are shown. Here we depict only the imaginary parts, i.e.,  $\tilde{\Delta}(\omega) = -\text{Im}\Delta(\omega)/\pi$ . Due to the spin-orbit coupling effect, the hybridization functions are split into two parts,  $5f_{5/2}$  and  $5f_{7/2}$  components. We can see that there are exactly strong hybridizations between the  $5f$  bands and the other bands below the Fermi level. The  $c$ - $f$  hybridization in the Cm(III) case is slightly weaker than the others. Strong  $c$ - $f$  hybridization enables the valence electrons to transfer between  $5f$  and  $spd$  bands and finally leads to the so-called mixed-valence or valence state fluctuation behavior as discussed below.

## C. Valence state fluctuations

Valence state fluctuation is a ubiquitous feature in strongly correlated  $f$ -electron systems [25,45,46]. It is very sensitive to

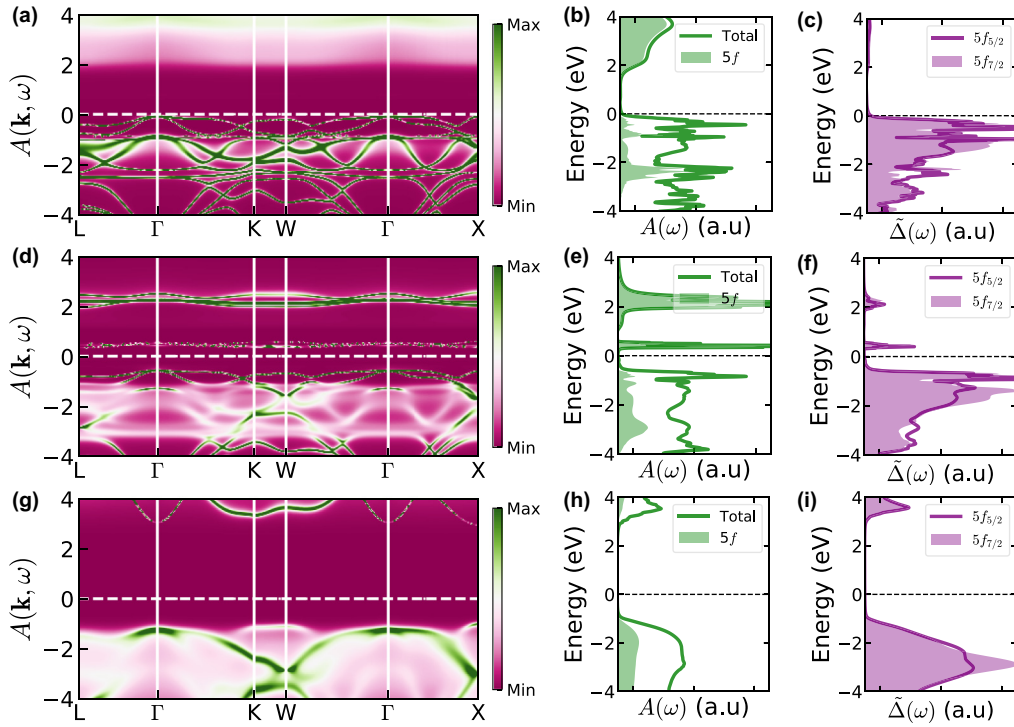


FIG. 2. Ground-state electronic structure of  $\text{CmO}_2$  obtained by the DFT + DMFT method. The results for the Cm(IV) configuration ( $n_{5f}^0 = 6.0$ ) are shown in (a)–(c), while those for the Cm(III) configuration ( $n_{5f}^0 = 7.0$ ) are shown in (g)–(i). The results shown in (d)–(f) are for the intermediate configuration ( $n_{5f}^0 = 6.5$ ). (a), (d), and (g) Momentum-resolved spectral functions  $A(\mathbf{k}, \omega)$ . (b), (e), and (h) Total density of states (thick solid lines) and  $5f$  partial density of states (colored shaded areas). (c), (f), and (i) Imaginary parts of hybridization functions. The  $5f_{5/2}$  and  $5f_{7/2}$  manifolds are represented by solid lines and colored shaded areas, respectively. The horizontal dashed lines denote the Fermi level.

external conditions, such as temperature, pressure, alloying, etc. [37,47–49]. Naturally, we expected that valence state fluctuation behaviors should be quite different for the Cm(III), intermediate-configuration, and Cm(IV) cases. The valence state histogram may be the most suitable quantity to qualify the valence state fluctuation. It denotes the probability of finding a valence electron in a given atomic eigenstate  $|\psi_\Gamma\rangle$ , which is labeled by using some good quantum numbers (such as total occupancy  $N$  and total angular momentum  $J$ ) [25,35]. Thus, we tried to calculate this physical quantity via the CT-HYB quantum impurity solver [24,34]. The calculated results are illustrated in Fig. 3. (i) For the Cm(IV) case, the valence state fluctuation is rather weak [see Fig. 3(a)]. The predominant atomic eigenstate is  $|N = 6.0, J = 0.0, \gamma = 0.0\rangle$ . It accounts for approximately 70%. The residual contributions are mainly from the atomic eigenstates with  $N = 7$ . Although the contributions from the other high-lying atomic eigenstates are quite small, they are not trivial and have to be taken into consideration explicitly. (ii) As for the Cm(III) case, it manifests the weakest valence state fluctuation [see Fig. 3(g)]. The atomic eigenstate  $|N = 7.0, J = 3.5, \gamma = 0.0\rangle$  becomes overwhelming. It accounts for approximately 90%, which means the  $5f$  electrons are virtually locked at this atomic eigenstate (the ground state). The contributions from the other atomic eigenstates are indeed trivial. (iii) For the intermediate configuration, we observe heavy  $5f$  valence state fluctuation [see Fig. 3(d)]. There are at least three atomic eigenstates ( $|N = 6, J = 0, \gamma = 0\rangle$ ,  $|N = 7, J = 3.5, \gamma = 0\rangle$ , and  $|N =$

$7, J = 3.5, \gamma = 1\rangle$ ), whose contributions are comparable. (iv) Finally, from the perspective of valence state fluctuation, we have the intermediate configuration  $> \text{Cm(IV)} > \text{Cm(III)}$ . The strong  $c$ - $f$  hybridization may be the driving force of  $5f$  valence state fluctuation.

The distributions of valence electron configurations are summed up and shown in Fig. 3. Clearly, these systems are mixed valence. For the Cm(IV) case, it is a mixture of  $5f^{5.0}$ ,  $5f^{6.0}$ , and  $5f^{7.0}$  electronic configurations [see Fig. 3(b)]. As a consequence, its effective  $5f$  occupancy  $\langle N_{5f} \rangle$  is about 6.26. As for the Cm(III) case, its ground state comprises  $5f^{6.0}$ ,  $5f^{7.0}$ , and  $5f^{8.0}$  electronic configurations [see Fig. 3(h)], so  $\langle N_{5f} \rangle \approx 7.06$ . Similarly, we find that  $\langle N_{5f} \rangle \approx 6.52$  for the intermediate configuration [see Fig. 3(e)]. The relationship between  $n_{5f}^0$  and  $\langle N_{5f} \rangle$  is shown in Fig. 1.

As a by-product, we can use the information on valence state fluctuation to make a rough estimation of the effective magnetic moment. Our strategy is as follows. First of all, we use the following equation to evaluate the expected value of a given quantum-mechanical operator  $A$ :

$$\langle A \rangle = \sum_{\Gamma} p_{\Gamma} A_{\Gamma}, \quad (2)$$

where  $p_{\Gamma}$  is the probability of any atomic eigenstate  $|\psi_{\Gamma}\rangle$  and  $\langle A \rangle$  could be  $\langle N_{5f} \rangle$ ,  $\langle J \rangle$ ,  $\langle L \rangle$ , and  $\langle S \rangle$ . Next, we can calculate

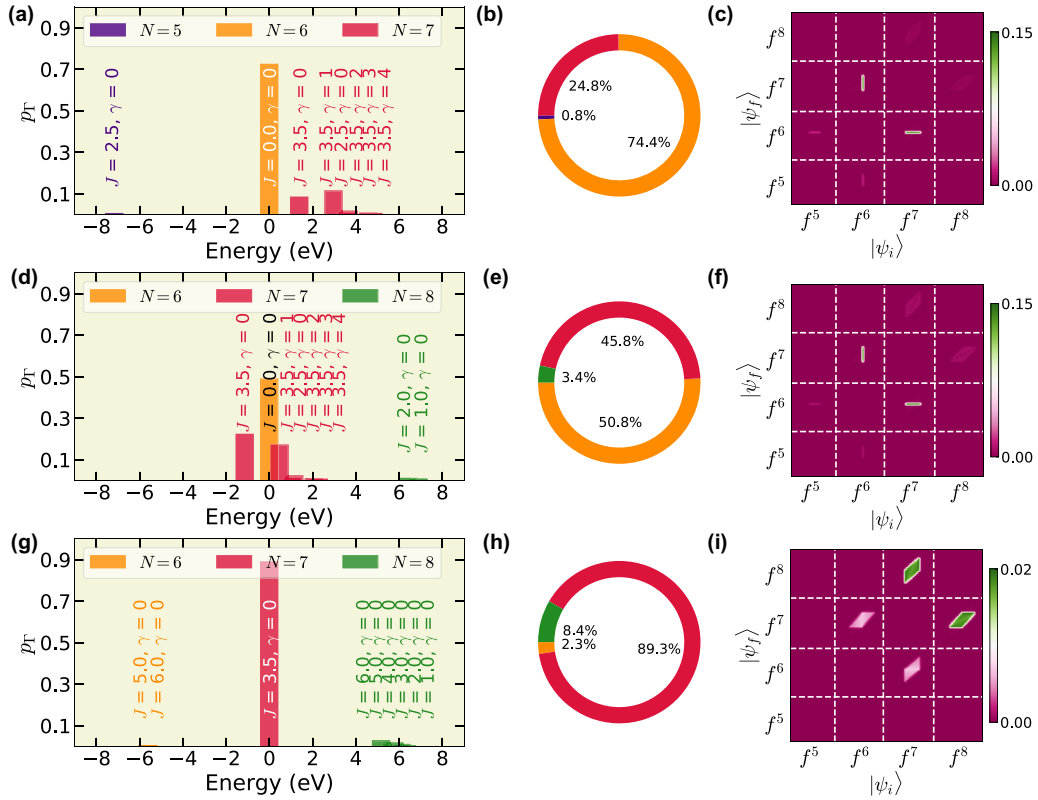


FIG. 3. Valence state fluctuations in  $\text{CmO}_2$  obtained by the DFT + DMFT method. The results for the Cm(IV) configuration ( $n_{5f}^0 = 6.0$ ) are shown in (a)–(c), while those for the Cm(III) configuration ( $n_{5f}^0 = 7.0$ ) are shown in (g)–(i). The results shown in (d)–(f) are for the intermediate configuration ( $n_{5f}^0 = 6.5$ ). (a), (d), and (g) Valence state histogram (or, equivalently, atomic eigenstate probability). Here the atomic eigenstates are labeled by using three good quantum numbers, namely,  $N$  (total occupancy),  $J$  (total angular momentum), and  $\gamma$  ( $\gamma$  stands for the combination of the rest of good quantum numbers). Most of the atomic eigenstates with trivial contributions are not shown in these panels. (b), (e), and (h) Distribution of atomic eigenstates with respect to total occupancy  $N$ . (c), (f), and (i) Transition probabilities between any two atomic eigenstates. Here  $|\psi_i\rangle$  and  $|\psi_f\rangle$  denote the initial and final states, respectively.

the Landé  $g$  factor  $g_J$  through

$$\langle g_J \rangle = \frac{3}{2} + \frac{\langle S \rangle (\langle S \rangle + 1) - \langle L \rangle (\langle L \rangle + 1)}{2 \langle J \rangle (\langle J \rangle + 1)}. \quad (3)$$

Finally, the effective magnetic moment  $\mu_{\text{eff}}$  can be calculated via the following relation [50]:

$$\mu_{\text{eff}} \approx \langle g_J \rangle \sqrt{\langle J \rangle (\langle J \rangle + 1)}. \quad (4)$$

The calculated results are summarized in Fig. 4.

For the Cm(IV) case,  $\langle J \rangle \approx 0.96$ ,  $\langle L \rangle \approx 2.71$ , and  $\langle S \rangle \approx 2.83$ . For the Cm(III) case,  $\langle J \rangle \approx 3.59$ ,  $\langle L \rangle \approx 0.34$ , and  $\langle S \rangle \approx 3.44$ . All these values deviate apparently from the values at atomic limits. In the case where  $n_{5f}^0$  goes from 6.0 to 7.0, we can split this process into three distinct stages according to the changes in  $\langle J \rangle$  and  $\mu_{\text{eff}}$ . (i) When  $n_{5f}^0 < 6.6$ ,  $\langle J \rangle$  and  $\mu_{\text{eff}}$  increase monotonously with respect to  $n_{5f}^0$ . Further, we find that  $\langle J \rangle - n_{5f}^0$  and  $\mu_{\text{eff}} - n_{5f}^0$  exhibit quasilinear relations. (ii) When  $6.6 < n_{5f}^0 < 6.7$ , sudden jumps for  $\langle J \rangle$  and  $\mu_{\text{eff}}$  are discerned. It is speculated that a magnetic or electronic transition would occur here. (iii) When  $n_{5f}^0 > 6.7$ ,  $\langle J \rangle$  and  $\mu_{\text{eff}}$  approach their saturated values,  $3.60\mu_B$  and  $8.0\mu_B$ , respectively. Notice that the Landé  $g$  factor remains almost constant during this process ( $\langle g_J \rangle \approx 2.0$ ). From the calculated and experimental values of  $\mu_{\text{eff}}$ , we can conclude that the oxidation state of Cm

ions in  $\text{CmO}_2$  is neither Cm(III) nor Cm(IV) [15,17]. It should be an intermediate configuration. In Fig. 4(b), the possible oxidation states are highlighted by the pink region. We have  $6.2 < n_{5f}^0 < 6.5$  and the corresponding  $5f$  occupancy  $6.35 < \langle n_{5f} \rangle < 6.52$  (see Fig. 1).

In Fig. 3, we also plot the transition probabilities between any two atomic eigenstates  $\Pi(\langle \psi_f | \psi_i \rangle)$ . Here  $|\psi_i\rangle$  and  $|\psi_f\rangle$  denote the initial and final states, respectively. We can see intense many-body transitions between  $5f^{6.0}$  and  $5f^{7.0}$  states for the Cm(IV) case [see Fig. 3(c)] and the intermediate configuration [see Fig. 3(f)]. For the Cm(III) case, the transitions between  $5f^{7.0}$  and  $5f^{8.0}$  states become dominant [see Fig. 3(i)]. Overall, the intermediate configuration exhibits stronger and more centralized many-body transitions. In the Cm(IV) case, although the magnetic excited states (i.e., the  $5f^{7.0}$  states) exist, their contributions are not sufficient to reproduce the experimentally observed magnetic moment [15].

#### D. Spin-spin correlation functions

To gain a deeper understanding of the magnetic properties of  $\text{CmO}_2$ , we further examine its imaginary-time spin-spin correlation functions  $\chi(\tau)$ ,

$$\chi(\tau) = \langle S_z(\tau) S_z(0) \rangle. \quad (5)$$

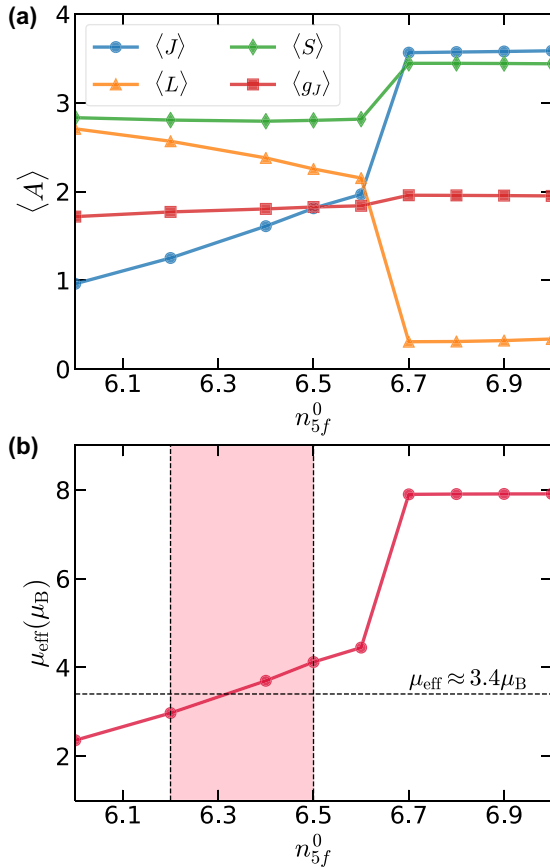


FIG. 4. (a) Effective total angular momentum  $\langle J \rangle$ , orbital momentum  $\langle L \rangle$ , spin momentum  $\langle S \rangle$ , and Landé  $g$  factor  $\langle g_J \rangle$  as a function of  $n_{5f}^0$ . (b) Effective local magnetic moment  $\mu_{\text{eff}}$  as a function of  $n_{5f}^0$ . The experimental value, which is denoted by a horizontal dashed line, is taken from Ref. [15]. Here the pink region marks the most likely oxidation oxides of Cm ions ( $n_{5f}^0 \in [6.2, 6.5]$ ). Their local magnetic moments are plausible and close to the experimental value.

At first, we used the CT-HYB quantum impurity solver to measure the local dynamical susceptibility  $\chi$  as a function of Matsubara frequencies  $i\omega_n$  [24,35]. Later, we converted it into an imaginary-time axis to obtain  $\chi(\tau)$ ,

$$\chi(\tau) = \frac{1}{\beta} \sum_n e^{-i\omega_n \tau} \chi(i\omega_n). \quad (6)$$

The calculated results for  $\chi(\tau)$  are illustrated in Fig. 5. We find that the asymptotic behaviors of  $\chi(\tau)$  for various  $n_{5f}^0$  are totally different. (i) When  $n_{5f}^0 < 6.6$ ,  $\chi(\tau)$  approaches zero very quickly. (ii) When  $n_{5f}^0 = 6.6$ ,  $\chi(\tau)$  decreases slowly and finally goes to a small, finite value at large  $\tau$ . (iii) When  $n_{5f}^0 > 6.6$ ,  $\chi(\tau)$  drops almost immediately and then starts to remain at a large fixed value at small  $\tau$ . These facts suggest that  $\text{CmO}_2$  will fall into a spin-freezing-like phase [51] once  $n_{5f}^0 \geq 6.6$ . This conclusion is consistent with the evolution of  $\mu_{\text{eff}}$  with respect to  $n_{5f}^0$  [see Fig. 4(b)].

Actually, we can use the following equation to evaluate the effective local magnetic moment  $\mu_{\text{eff}}$  again [52]:

$$\mu_{\text{eff}} = \sqrt{T \chi_{\text{loc}}}, \quad (7)$$

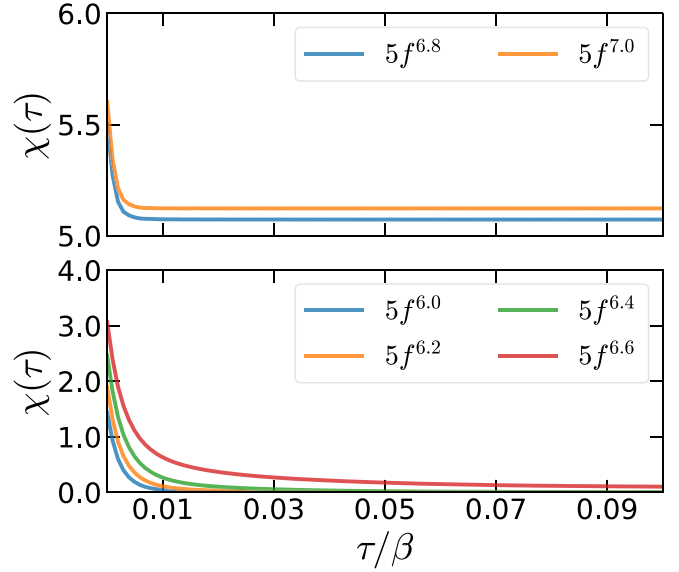


FIG. 5. Imaginary-time spin-spin correlation functions of  $\text{CmO}_2$ ,  $\chi(\tau) = \langle S_z(\tau)S_z(0) \rangle$ . Top: For low-oxidation states of Cm ions ( $n_{5f}^0 = 6.8$  and  $7.0$ ). Bottom: For high-oxidation states of Cm ions ( $n_{5f}^0 = 6.0, 6.2, 6.4, \text{ and } 6.6$ ).

where  $\chi_{\text{loc}}$  is defined as

$$\chi_{\text{loc}} = \int_0^\beta d\tau \chi(\tau). \quad (8)$$

Using the data presented in Fig. 5, we reevaluated  $\mu_{\text{eff}}$  as a function of  $n_{5f}^0$ . These values are smaller than those obtained via distributions of atomic eigenstates, but the overall trend is entirely similar. We confirm again that there will be a leap for  $\mu_{\text{eff}}$  when  $6.6 < n_{5f}^0 < 6.7$ . Only the intermediate configuration can yield a plausible local magnetic moment.

#### IV. DISCUSSION

*Puzzling magnetic behaviors in  $\text{CmO}_2$ .* As mentioned before, a few mechanisms have been proposed to explain the puzzling magnetic properties in  $\text{CmO}_2$ . Here we would like to summarize and compare their successes and failures.

(i) *Pure Cm(IV) ions.* This explanation is incorrect because it yields a nonmagnetic ground state. Even if we consider the effect of valence state fluctuation, the resulting magnetic moment is too small. Petit *et al.* employed the self-interaction corrected local spin-density approximation (SIC-LSD) to study the electronic structures and magnetic properties of  $\text{CmO}_2$  as well [40]. They assumed that the initial configuration of Cm ions is Cm(IV). However, due to the spin-orbit coupling and hybridization, this initial configuration is significantly distorted, and in fact, the orbital moment is almost quenched (the spin moment is retained). Thus, a finite magnetic moment is obtained ( $\mu_{\text{eff}} \approx 5.21 \mu_B$ ). This explanation sounds somewhat reasonable. But the resulting  $5f$  occupancy is about 6.86, which is far from the  $5f^{6.0}$  or  $5f^{7.0}$  configuration.

(ii) *Pure Cm(III) ions.* This explanation is excluded as well because it overestimates the magnetic moment.

(iii) *A mixture of Cm(IV) and Cm(III) ions.* This mechanism sounds reasonable. It can generate rational magnetic moment,

but it requires rearrangement of the oxygen sublattice. In other words, one way to satisfy the  $\text{Cm}^{3+}$  valence and  $\text{O}^{2-}$  configuration at the same time would be to take the sesquioxide ( $\text{Cm}_2\text{O}_3$ ), which is not supported by the neutron diffraction experiment [15].

(iv) *Cm(IV) ions in excited states.* This mechanism is restricted by temperature. In the low-temperature region, it becomes invalid.

(v) *Covalent picture or intermediate configuration.* The spirit of this explanation is twofold. At first, Cm can borrow additional electrons from O  $2p$  orbitals via the covalent bonds [19] or the mechanism of  $c$ - $f$  hybridization. Previous calculations using screened hybrid density functional theory revealed that the charge densities at oxygen sites deviate apparently from the expected values ( $\text{O}^{2-}$ ) [19]. Actually, in our DFT + DMFT calculations, we find that  $\langle N_{\text{O}_{2p}} \rangle$  is about 4.5 for  $n_{5f}^0 = 6.5$ . This means that the O ions in  $\text{CmO}_2$  probably do not form closed shells. Second, Cm's  $5f$  electrons could spend quite a lot of their lifetime in the atomic eigenstates with  $N = 7$  and  $N = 8$  due to the strong valence state fluctuation, leading to a finite macroscopic moment. This mechanism does not break the cubic crystal symmetry. It is not sensitive to the change in temperature. More important, it is consistent with all the available experimental results [15–17,44]. Therefore, we believe that the intermediate configuration is more reasonable for the ground-state electronic structure of  $\text{CmO}_2$ .

*Abnormal lattice constants in  $\text{CmO}_2$ .* The intermediate configuration also provides a possible explanation for the abnormal lattice constants in  $\text{CmO}_2$ . The formal valence of Cm ions in  $\text{CmO}_2$  is +4. However, according to the present calculated results, its valence is noninteger and exhibits a significant trend toward +3. As for  $\text{AmO}_2$  and the early members of  $\text{AO}_2$ , the formal expectations, i.e.,  $A^{4+}$ , are well satisfied [19]. Therefore, it is easy to understand why the lattice constants of  $\text{CmO}_2$  deviate from the general trend and show an evident cusp in the plot of  $a_0 - Z$  for  $\text{AO}_2$ . Actually, sesquioxides are more stable than dioxides for the late members of the actinide series. For actinides beyond Cf, only the sesquioxides have been observed experimentally [53,54]. Clearly,  $\text{CmO}_2$  sits at the boundary between  $A^{3+}$  and  $A^{4+}$ .

*Temperature- and pressure-dependent electronic structures.* We further examine the temperature dependence and pressure dependence of  $5f$  electronic configurations in  $\text{CmO}_2$ . The Cm(III) and Cm(IV) cases are taken as two representative examples. We find that the two oxidation states are quite stable against temperature and volume compression. In Fig. 6, the calculated  $5f$  occupancies as functions of temperature and volume are shown. Clearly,  $\langle N_{5f} \rangle$  remains almost constant if we take numerical fluctuations into considerations. If we further increase the pressure (or reduce the volume), what will happen? Notice that  $\text{CmO}_2$  will undergo a structural phase transition when the pressure is between 30 and 40 GPa.  $\text{CmO}_2$  will transform from the cubic phase (space group  $Fcc$ ) to the orthorhombic structure (space group  $Pnma$ ), with about 10% volume collapse [41]. Similar volume changes have been observed in the high-pressure phase transitions of other actinide dioxides (such as  $\text{AmO}_2$  and  $\text{UO}_2$ ) [55–57], which are likely linked to the  $5f$  localized-itinerant crossover. As for  $\text{CmO}_2$ , it is expected that the  $5f$  occupancy will decrease

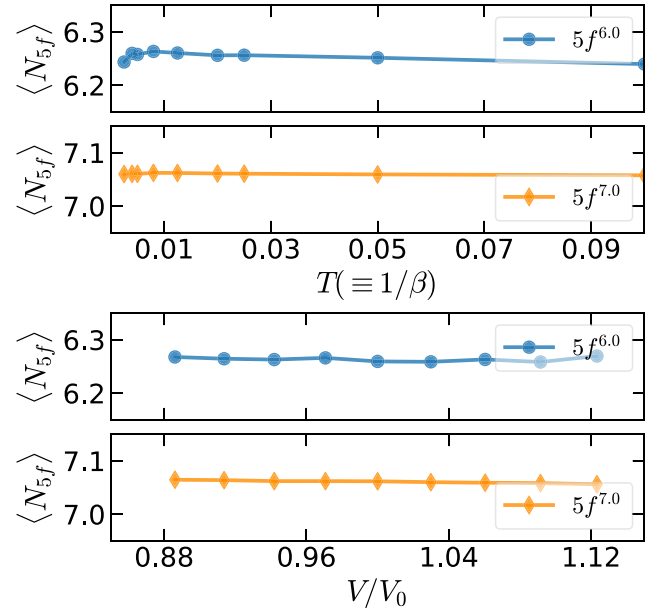


FIG. 6. Top: Temperature dependence of  $5f$  occupancies. Bottom: Volume (or pressure) dependence of  $5f$  occupancies. Here  $V_0 = 259.45 \text{ bohrs}^3$ .

(or, equivalently, the  $5f$  valence will increase,  $\text{Cm}^{3+} \rightarrow$  intermediate valence  $\rightarrow \text{Cm}^{4+}$ ) under pressure, and the local magnetic moment should be suppressed as well.

## V. CONCLUSIONS

In summary, we reported a systematic study of the ground-state electronic structure in  $\text{CmO}_2$ . We carried out fully charge self-consistent DFT + DMFT calculations and considered various possible oxidation states of Cm ions. Our major findings are as follows. First, the ground-state electronic configuration of Cm ions is neither Cm(III) nor Cm(IV). It should be an intermediate configuration. This configuration is very stable over a wide range of temperature or pressure. Second, the intermediate configuration leads to a macroscopic local moment in the nominally nonmagnetic  $\text{CmO}_2$  via the valence state fluctuation mechanism. The obtained  $5f$  occupancy is about 6.35–6.52. Third, we predict that  $\text{CmO}_2$  is a wide-gap charge transfer insulator (indirect band gap,  $E_{\text{gap}} > 1.0 \text{ eV}$ ). Further experiments to verify our predictions and proposals are highly needed. X-ray magnetic circular dichroism would be an ideal tool to detect the mixed-valence behaviors of Cm ions in  $\text{CmO}_2$  because it is extremely sensitive to the  $f^6$  and  $5f^7$  configurations and needs only microgram quantities for the experiments [4].

## ACKNOWLEDGMENTS

We thank Prof. G. Lander for fruitful discussions. This work was supported by the Natural Science Foundation of China (Grants No. 11874329, No. 11934020, and No. 11704347) and the Science Challenge Project of China (Grant No. TZ2016004).

### APPENDIX: DOUBLE-COUNTING TERM USED IN THE SIMULATION

In the framework of the DFT + DMFT approach, the double-counting term  $\Sigma_{\text{dc}}$  plays a pivotal role [26]. It is employed to cancel out the excess amount of the electronic correction effect that is included partly in the DFT part. Actually, it is used to evaluate the energy levels of correlated orbitals via the following equation [31]:

$$\epsilon_{\alpha}^{\text{imp}} = \epsilon_{\alpha}^{\text{DFT}} - \Sigma_{\text{dc},\alpha} - \mu, \quad (\text{A1})$$

where  $\alpha$  is the orbital index,  $\epsilon_{\alpha}^{\text{DFT}}$  is the energy level obtained by DFT, and  $\mu$  is the chemical potential. Since the occupation of the correlated orbital  $\alpha$  (i.e.,  $n_{\alpha}$ ) is a function of  $\epsilon_{\alpha}^{\text{imp}}$ , it depends on  $\Sigma_{\text{dc}}$  indirectly. In other words,  $n_{\alpha}$  can be tuned via the double-counting term.

To our knowledge, the exact expression for  $\Sigma_{\text{dc}}$  is still under debate. There are two frequently used approximations for  $\Sigma_{\text{dc}}$ : the around-mean field scheme and the fully localized limit (FLL) scheme.  $\text{CmO}_2$  is a correlated insulator. According to the literature, the FLL scheme is a reasonable

choice [32]. It reads

$$\Sigma_{\text{dc}} = U \left( n_{5f} - \frac{1}{2} \right) - \frac{J_{\text{H}}}{2} (n_{5f} - 1.0), \quad (\text{A2})$$

where  $U$  is the Coulomb repulsion interaction parameter,  $J_{\text{H}}$  is Hund's exchange interaction parameter, and  $n_{5f}$  is the total occupancy of correlated  $5f$  orbitals [please pay attention to the difference between Eqs. (1) and (A2)]. Here  $U$  and  $J_{\text{H}}$  are semiempirical parameters. They are 7.5 and 0.6 eV, respectively [1]. As for  $n_{5f}$ , we have two options. (i) First, we have to give an initial value to it (for example,  $n_{5f} = 6.0$  or 7.0). Then we let it be determined self-consistently in the DFT + DMFT iterations. (ii) We set  $n_{5f}$  to a "nominal" value  $n_{5f}^0$  and fix it during the DFT + DMFT iterations. The first tactic always leads to a metallic solution. On the contrary, the second tactic works quite well. It not only reproduces the insulating nature of  $\text{CmO}_2$  successfully but also generates the desired  $5f$  occupancy (see Fig. 1). This is the true reason why we chose the second tactic to build the double-counting term and control the total occupancy of correlated  $5f$  orbitals.

- 
- [1] K. T. Moore and G. van der Laan, *Rev. Mod. Phys.* **81**, 235 (2009).
- [2] L. Severin, M. S. S. Brooks, and B. Johansson, *Phys. Rev. Lett.* **71**, 3214 (1993).
- [3] J. C. Lashley, A. Lawson, R. J. McQueeney, and G. H. Lander, *Phys. Rev. B* **72**, 054416 (2005).
- [4] N. Magnani, R. Caciuffo, F. Wilhelm, E. Colineau, R. Eloirdi, J.-C. Griveau, J. Ruzs, P. M. Oppeneer, A. Rogalev, and G. H. Lander, *Phys. Rev. Lett.* **114**, 097203 (2015).
- [5] S. Heathman, R. G. Haire, T. Le Bihan, A. Lindbaum, M. Idiri, P. Normile, S. Li, R. Ahuja, B. Johansson, and G. H. Lander, *Science* **309**, 110 (2005).
- [6] B. Kanellakopoulos, A. Blaise, J. Fournier, and W. Müller, *Solid State Commun.* **17**, 713 (1975).
- [7] G. H. Lander, J.-C. Griveau, R. Eloirdi, N. Magnani, E. Colineau, F. Wilhelm, S. D. Brown, D. Wermeille, A. Rogalev, R. G. Haire, and R. Caciuffo, *Phys. Rev. B* **99**, 224419 (2019).
- [8] X.-D. Wen, R. L. Martin, T. M. Henderson, and G. E. Scuseria, *Chem. Rev.* **113**, 1063 (2013).
- [9] S. Carretta, P. Santini, R. Caciuffo, and G. Amoretti, *Phys. Rev. Lett.* **105**, 167201 (2010).
- [10] G. Amoretti, A. Blaise, R. Caciuffo, J. M. Fournier, M. T. Hutchings, R. Osborn, and A. D. Taylor, *Phys. Rev. B* **40**, 1856 (1989).
- [11] N. Magnani, S. Carretta, R. Caciuffo, P. Santini, G. Amoretti, A. Hiess, J. Rebizant, and G. H. Lander, *Phys. Rev. B* **78**, 104425 (2008).
- [12] P. Santini, S. Carretta, G. Amoretti, R. Caciuffo, N. Magnani, and G. H. Lander, *Rev. Mod. Phys.* **81**, 807 (2009).
- [13] H. Yasuoka, G. Koutroulakis, H. Chudo, S. Richmond, D. K. Veirs, A. I. Smith, E. D. Bauer, J. D. Thompson, G. D. Jarvinen, and D. L. Clark, *Science* **336**, 901 (2012).
- [14] M.-T. Suzuki, N. Magnani, and P. M. Oppeneer, *Phys. Rev. B* **88**, 195146 (2013).
- [15] L. Morss, J. Richardson, C. Williams, G. Lander, A. Lawson, N. Edelstein, and G. Shalimoff, *J. Less-Common Met.* **156**, 273 (1989).
- [16] K. O. Kvashnina, S. M. Butorin, D. K. Shuh, J.-H. Guo, L. Werme, and J. Nordgren, *Phys. Rev. B* **75**, 115107 (2007).
- [17] S. E. Nave, R. G. Haire, and P. G. Huray, *Phys. Rev. B* **28**, 2317 (1983).
- [18] F. Niikura and T. Hotta, *Phys. Rev. B* **83**, 172402 (2011).
- [19] I. D. Prodan, G. E. Scuseria, and R. L. Martin, *Phys. Rev. B* **76**, 033101 (2007).
- [20] L. R. Morss, J. Fuger, and N. M. Edelstein, *The Chemistry of the Actinide and Transactinide Elements* (Springer, Dordrecht, 2006).
- [21] L. B. Asprey, F. H. Ellinger, S. Fried, and W. H. Zachariasen, *J. Am. Chem. Soc.* **77**, 1707 (1955).
- [22] J. Peterson and J. Fuger, *J. Inorg. Nucl. Chem.* **33**, 4111 (1971).
- [23] L. Hou, W.-D. Li, F. Wang, O. Eriksson, and B.-T. Wang, *Phys. Rev. B* **96**, 235137 (2017).
- [24] E. Gull, A. J. Millis, A. I. Lichtenstein, A. N. Rubtsov, M. Troyer, and P. Werner, *Rev. Mod. Phys.* **83**, 349 (2011).
- [25] J. H. Shim, K. Haule, and G. Kotliar, *Nature (London)* **446**, 513 (2007).
- [26] G. Kotliar, S. Y. Savrasov, K. Haule, V. S. Oudovenko, O. Parcollet, and C. A. Marianetti, *Rev. Mod. Phys.* **78**, 865 (2006).
- [27] A. Georges, G. Kotliar, W. Krauth, and M. J. Rozenberg, *Rev. Mod. Phys.* **68**, 13 (1996).
- [28] P. Blaha, K. Schwarz, G. Madsen, D. Kvasnicka, and J. Luitz, *WIEN2k, an Augmented Plane Wave + Local Orbitals Program for Calculating Crystal Properties*, edited by K. Schwarz (Technische Universität Wien, Vienna, 2001).
- [29] R. Konings, *J. Nucl. Mater.* **298**, 255 (2001).
- [30] J. P. Perdew, K. Burke, and M. Ernzerhof, *Phys. Rev. Lett.* **77**, 3865 (1996).
- [31] K. Haule, C.-H. Yee, and K. Kim, *Phys. Rev. B* **81**, 195107 (2010).



- [32] V. I. Anisimov, F. Aryasetiawan, and A. I. Lichtenstein, *J. Phys.: Condens. Matter* **9**, 767 (1997).
- [33] Here we establish the maps between Cm(IV) and  $n_{5f}^0 = 6.0$  and between Cm(III) and  $n_{5f}^0 = 7.0$ . However, when  $n_{5f}^0 = 6.0$ , the resulting  $5f$  occupancy  $\langle N_{5f} \rangle$  is about 6.26, instead of 6.0 (see Fig. 1). The situation is similar for the  $n_{5f}^0 = 7.0$  case.
- [34] P. Werner, A. Comanac, L. de' Medici, M. Troyer, and A. J. Millis, *Phys. Rev. Lett.* **97**, 076405 (2006).
- [35] K. Haule, *Phys. Rev. B* **75**, 155113 (2007).
- [36] The ordering of CmO<sub>2</sub> is not expected and has not been found by susceptibility measurements, at least down to about 3 K.
- [37] L. Huang and H. Lu, *Phys. Rev. B* **99**, 045109 (2019).
- [38] S. Y. Savrasov, K. Haule, and G. Kotliar, *Phys. Rev. Lett.* **96**, 036404 (2006).
- [39] F. Birch, *Phys. Rev.* **71**, 809 (1947).
- [40] L. Petit, A. Svane, Z. Szotek, W. M. Temmerman, and G. M. Stocks, *Phys. Rev. B* **81**, 045108 (2010).
- [41] J. Dancausse, R. Haire, S. Heathman, and U. Benedict, *J. Nucl. Sci. Technol.* **39**, 136 (2002).
- [42] L. de' Medici, J. Mravlje, and A. Georges, *Phys. Rev. Lett.* **107**, 256401 (2011).
- [43] J. T. Pegg, X. Aparicio-Anglès, M. Storr, and N. H. de Leeuw, *J. Nucl. Mater.* **492**, 269 (2017).
- [44] B. W. Veal, D. J. Lam, H. Diamond, and H. R. Hoekstra, *Phys. Rev. B* **15**, 2929 (1977).
- [45] C.-H. Yee, G. Kotliar, and K. Haule, *Phys. Rev. B* **81**, 035105 (2010).
- [46] M. Janoschek, P. Das, B. Chakrabarti, D. L. Abernathy, M. D. Lumsden, J. M. Lawrence, J. D. Thompson, G. H. Lander, J. N. Mitchell, S. Richmond, M. Ramos, F. Trouw, J.-X. Zhu, K. Haule, G. Kotliar, and E. D. Bauer, *Sci. Adv.* **1**, e1500188 (2015).
- [47] H. Lu and L. Huang, *Phys. Rev. B* **94**, 075132 (2016).
- [48] H. Lu and L. Huang, *Phys. Rev. B* **98**, 195102 (2018).
- [49] L. Huang and H. Lu, *Phys. Rev. B* **99**, 045122 (2019).
- [50] T. Gouder, G. van der Laan, A. B. Shick, R. G. Haire, and R. Caciuffo, *Phys. Rev. B* **83**, 125111 (2011).
- [51] P. Werner, E. Gull, M. Troyer, and A. J. Millis, *Phys. Rev. Lett.* **101**, 166405 (2008).
- [52] J. Kuneš, A. V. Lukoyanov, V. I. Anisimov, R. T. Scalettar, and W. E. Pickett, *Nat. Mater.* **7**, 198 (2008).
- [53] R. Haire, *J. Alloys Compd.* **223**, 185 (1995).
- [54] J. Moore, S. Nave, R. Haire, and P. G. Huray, *J. Less-Common Met.* **121**, 187 (1986).
- [55] M. Idiri, T. Le Bihan, S. Heathman, and J. Rebizant, *Phys. Rev. B* **70**, 014113 (2004).
- [56] L. Huang, Y. Wang, and P. Werner, *Europhys. Lett.* **119**, 57007 (2017).
- [57] S. Li, R. Ahuja, and B. Johansson, *High Pressure Res.* **22**, 471 (2002).